

Spectroscopic properties, anti-colon cancer, antimicrobial and molecular docking studies of silver(I), manganese(II), cobalt(II) and nickel(II) complexes for 2-amino-4-phenylthiazole derivative

Sami Abdullah Al-Harbi ¹, Mahmoud Sayed Bashandy ^{1,2}, Hamed Mohammed Al-Saidi ¹, Adel Abbas Ahmed Emara ^{3,*} and Shima Mohamed Abd El-Gilil ⁴

¹ Department of Chemistry, University College in Al-Jamoum, Umm Al-Qura University, 21955, Makkah, Saudi Arabia

² Department of Chemistry, Faculty of Science (Boys), Al-Azhar University, Nasr City, 11884, Cairo, Egypt

³ Department of Chemistry, Faculty of Education, Ain Shams University, Roxy, 11711, Cairo, Egypt

⁴ Department of Organic Chemistry, Faculty of Pharmacy (Girls), Al-Azhar University, Nasr City, 11754, Cairo, Egypt

* Corresponding author at: Department of Chemistry, Faculty of Education, Ain Shams University, Roxy, 11711, Cairo, Egypt. Tel.: +2.010.23131160. Fax: +2.02.24551530. E-mail address: adelaemara@yahoo.com (A.A.A. Emara).

ARTICLE INFORMATION



DOI: 10.5155/eurjchem.7.4.421-430.1490

Received: 20 August 2016

Received in revised form: 01 October 2016

Accepted: 02 October 2016

Published online: 31 December 2016

Printed: 31 December 2016

KEYWORDS

Thiazole
 Anti-colon cancer
 Schiff base ligand
 Molecular docking
 Binuclear complexes
 Antimicrobial activity

ABSTRACT

Thiazole Schiff base (H₂L) ligand was synthesized from condensation of 2-amino-4-phenylthiazole with 4,6-diacetylresorcinol in the molar ratio 2:1. A series of Ag(I), Mn(II), Co(II) and Ni(II) complexes of H₂L ligand was prepared and investigated by elemental analysis, IR, UV, ¹H NMR, TGA and mass spectral data. Thiazol Schiff base ligand has two bidentate sets of N-O units which can coordinate with two metal ions to afford novel binuclear metal complexes. The directions of the coordinate bonds are from nitrogen atoms of the azomethine groups and oxygen atoms of the phenolic groups. All of the newly synthesized complexes were evaluated for their antimicrobial activities. The results showed the Ag(I) complex exhibited better activities than the commercial antimicrobial reference drugs. The metal complexes were also evaluated for their *in-vitro* anti-colon human cancer (HCT-116) and mammalian cells of the African green monkey kidney (VERO). The Ag(I) and Co(II) complexes with selectivity index value 17.00 and 15.63, respectively, exhibited better activity than methotrexate as a reference drug with selectivity index value 13.30, while complexes Ni(II) and Mn(II) with selectivity index values 9.30 and 8.59, respectively, were found to be nearly as active as methotrexate. Molecular docking studies further helped in understanding the mode of action of the compounds through their various interactions with the active sites of the dihydrofolate reductase enzyme. The observed activity of the Ag(I), Mn(II) and Ni(II) complexes gave rise to the conclusion that they might exert their action through inhibition of the dihydrofolate reductase enzyme.

Cite this: *Eur. J. Chem.* **2016**, *7*(4), 421-430

1. Introduction

Recently, the development of antimicrobial and anticancer therapeutic agents has been paved the way to introduce both thiazole moieties and/or transition metal ions, which can avoid such side effects. Schiff base ligands play a central role as chelating ligands in transition metal coordination chemistry [1-3]. A bimetallic core is versatile at the active site of many metalloenzymes and plays an essential role in biological systems *via* the interplay of a pair of metal ions [4]. In the last two decades, a large number of bimetallic Schiff base complexes of different structural types have been synthesized and characterized [5,6]. These complexes vary in their new applications, of biological activities [7-11].

2-Amino-4-phenylthiazole and its Schiff base derivatives, which are formed by the condensation reaction with aldehydes and ketones showed significant antibacterial and antifungal and anticancer activities [12-15]. Additionally, the

same behaviors were also identified in the transition metal complexes of 2-amino-4-phenylthiazole derivatives [16-19].

In our previous published work [20], we managed to get a number of transition metal complexes with ligand contains thiazole group and study their anti-microbial and anti-cancer tumors effects. In extension to this work in our laboratory, we have succeeded to synthesize Ag(I), Mn(II), Co(II) and Ni(II) thiazole Schiff base ligand. Anti-microbial and anti-cancer studies were investigated.

In the present study, the thiazole Schiff base, H₂L, ligand was prepared by the condensation of 4,6-diacetylresorcinol, as a starting material, with 2-amino-4-phenylthiazole as cited in the literature [20]. The reaction of this ligand with silver(I), nickel(II), cobalt(II), and manganese(II) ions, in the 1:2 molar ratio (ligand : metal ion) were studied. The newly prepared metal complexes of this ligand were identified by different physicochemical and spectroscopic techniques.

The Schiff base, H₂L, ligand and its metal complexes were investigated for antibacterial and antifungal properties. Eight

pathogenic microorganisms were used for this investigation. The Gram-positive bacteria used were *Staphylococcus aureus* (RCMB 010027), *Streptococcus pneumoniae* (RCMB 010010) and *Bacillus subtilis* (RCMB 010067). The Gram-negative bacteria were *Pseudomonas aeruginosa* (RCMB 010043), *Klebsiella pneumoniae* (RCMB 0010093) and *Escherichia coli* (RCMB 010052). Two fungi, *Aspergillus fumigatus* (RCMB 02568) and *Candida albicans* (RCMB 05036), were also utilized.

Currently, colorectal cancer is the third most commonly diagnosed cancer in males worldwide and the fourth most common in females. Thiazole Schiff base ligands and their metal complexes are one of the drugs involved in the cytotoxicity of anticancer. Therefore, this present work is considered an assessment where the transition metal complexes of a Schiff base containing sulfur is overcoming the human cancer colon carcinoma HCT-116 cell line.

2. Experimental

2.1. Materials

Thiazole Schiff base, H₂L, ligand was synthesized according to the methods specified in the literature [20]. Silver(I), manganese(II), cobalt(II) and nickel(II) ions were used as nitrate salts and were Merck or BDH. Organic solvents (absolute ethanol, methanol, diethyl ether and dimethyl formamide) were obtained from Sigma-Aldrich and were used as supplied.

2.2. Synthesis of Schiff base ligand

The ligand was synthesized by adding 4,6-diacetyl resorcinol (DAR) (3.88 g, 20 mmol) dissolved in hot absolute ethanol (30 mL) to 2-amino-4-phenylthiazole (APT) (7.04 g, 40 mmol) in absolute ethanol (30 mL). The reaction mixture was heated to reflux for 4 h. Yellow crystals were filtered off and washed with a few amount of ethanol then ether and air dried. Fine crystals were obtained by recrystallization from ethanol. Color: Yellow. Yield: 7.98 g (78.2%). M.p.: 212-213 °C. FT-IR (KBr, ν , cm^{-1}): 3400-3166 (OH) (br, alcohol), 3050 (CH-aromatic), 2990 (CH-aliphatic) 1629 (C=N). ¹H NMR (400 MHz, DMSO-*d*₆, δ , ppm): 2.14 (s, 6H, 2CH₃), 5.37 (s, 2H, 2OH; discharged with D₂O), 7.28 (s, 2H, 2CH-thiazole-H₅), 6.41-8.23 (m, 12H, Ar-H). MS (EI, m/z (%)): 512 (M⁺+2, 100). Anal. calcd. for C₂₈H₂₂N₄O₂S₂: C, 65.86; H, 4.34; N, 10.97. Found: C, 65.84; H, 4.21; N, 11.00%. UV/Vis (DMF, λ_{max} , nm, (ϵ)): 272 (7.31), 324 (8.34), 335 (4.48), 417 (5.53). $n_D^{25} = 1.381$. $[\alpha]_D^{25} = -67.6$ (c 0.6, DMF). Λ_m (S.m².mol⁻¹): 14.

2.3. Synthesis of transition metal complexes of the Schiff base (H₂L) ligand

The mixtures of the H₂L ligand (2.55 g; 5.0 mmol) with metal salts (10 mmol) in 50 mL ethanol were stirred on cold for 30 minutes and then heated to reflux, for 3 hrs. The resulting precipitates were formed on cold after evaporation until near dryness. The products were filtered off, washed with ethanol and ether, and then air dried. The complexes are soluble in most common solvents. The obtained products were identified by IR spectra, MS and electronic spectra. The following detailed preparation is given as an example and the other complexes were obtained similarly.

2.3.1. Synthesis of Ni(II) complex

A solution of the H₂L ligand (2.55 g, 5.0 mmol) in ethanol (25 mL) was added gradually with constant stirring to Ni(NO₃)₂·6H₂O, (2.907 g, 10 mmol) in ethanol (25 mL). The pH of the mixture was 2.4. The mixture was stirred on cold for 30 min and then heated to reflux for 3 hrs. A yellow precipitate

was formed on cold after evaporation of the solvent on a water bath near dryness. Color: Yellow. Yield: 5.35 g (59.8%). M.p.: 177-178 °C. FT-IR (KBr, ν , cm^{-1}): 3380-3315 (OH) (br, alcohol), 3100 (CH-aromatic), 2930 (CH-aliphatic), 1742, 1383, 855 (NO₃⁻) (ionic), 579 (Ni-O), 459 (Ni-N). MS (EI, m/z (%)): 892 (M⁺, 100). Anal. calcd. for C₂₈H₃₆Ni₂N₆O₁₆S₂: C, 37.61; H, 4.06; N, 9.40; S, 7.17; Ni, 13.13. Found: C, 37.55; H, 4.11; N, 9.44; S, 7.27; Ni, 13.22%. UV/Vis (DMF, λ_{max} , nm, (ϵ)): 272 (8.72), 315 (7.44), 335 (4.92), 412 (4.34), 625 (5.74), 1000 (0.83). $n_D^{25} = 1.917$. $[\alpha]_D^{25} = +23.25$ (c 0.6, DMF). Λ_m (S.m².mol⁻¹): 145.

2.4. Physical measurements

Analysis of metal ions after the dissolution of the solid complex in hot concentrated nitric acid, HNO₃, then diluting with distilled water and filtering to remove the precipitated ligand. The solution was neutralized with ammonia solution and the metal ions were then titrated with EDTA using either murexide or Eriochrome Black T indicators [21-23]. Carbon, hydrogen, nitrogen and sulfur contents were carried out at the Microanalytical Center, Cairo and Al-Azhar University. The FT-IR spectra (4000-400 cm^{-1}) of the compounds were recorded as KBr discs using FT-IR (Shimadzu) spectrophotometer model 8400. Electronic spectra of the ligand and its metal complexes were carried out in 1×10⁻³ M DMF solution on an Angstrom UV-Vis spectrophotometer model 1100, in the range 200-1100 nm. Samples were introduced directly to the probe and the fragmentations were carried out at 300 °C and 70 eV. Magnetic susceptibilities of the complexes were measured by the Gouy method at room temperature using a magnetic susceptibility balance (Johnson Matthey, Alfa product, Model No. MKI). Effective magnetic moments were calculated from the expression $\mu_{\text{eff}} = 2.828 (\chi_M T)^{1/2}$ B.M., where χ_M is the molar susceptibility corrected using Pascal's constants for the diamagnetism of all atoms in the compounds and T is the absolute temperature [24]. Molar conductance of the solutions in mmoles of the solid complexes in DMF were measured on pH and conductmeter Instrument model 14831 (Italy). Melting points were not corrected and were measured by using a Stuart melting point instrument. Thermal gravimetric analysis (TGA) data was measured from room temperature to 800 °C at a heating rate 20 °C/min in dynamic N₂ atmosphere. The data were obtained using a Shimadzu TGA-50H instrument. Thermal analyzer equipped with a thermo-balance. The sample was contained in a boat shaped platinum pan suspended in the centre of a furnace.

2.5. Antimicrobial studies

The *in vitro* evaluation of antibacterial and antifungal activities was performed using standardized disc-agar diffusion method [25]. The activity of the synthesized compounds was determined against the following sensitive organisms: *Staphylococcus aureus* (RCMB 010027), *Streptococcus pneumoniae* (RCMB 010010) and *Bacillus subtilis* (RCMB 010067) as Gram-positive bacteria; *Pseudomonas aeruginosa* (RCMB 010043), *Klebsiella pneumoniae* (RCMB 0010093) and *Escherichia coli* (RCMB 010052) as Gram-negative bacteria; and *Aspergillus fumigatus* (RCMB 02568) and *Candida albicans* (RCMB 05036).

The antibiotic ampicillin was used as standard reference in the case of the Gram-positive bacteria, gentamicin was used as standard reference with the Gram-negative bacteria and amphotericin B was used as the standard antifungal reference control. The tested compounds were dissolved in DMF (which has no inhibition activity) to obtain concentrations of 5 mg/mL and 1 mg/mL. The test was performed on medium potato dextrose agar (PDA), which contains an infusion of 200 g potatoes, 6 g dextrose and 15 g agar [26,27].

Table 1. Physical and analytical data of the metal complexes of H₂L ligand.

No	Compound	Molecular formula	Yield (%)	Colour	M.p. (°C)	Elemental analyses; Calcd. (Found) %				
						C	H	N	S	M
1	[Ag ₂ (L)(H ₂ O) ₄]	C ₂₈ H ₂₈ Ag ₂ N ₄ O ₆ S ₂	71.3	Pale brown	172-173	42.23 (42.19)	3.54 (3.51)	7.04 (6.98)	8.05 (8.54)	27.09 (27.11)
2	[Mn ₂ (L)(H ₂ O) ₆](NO ₃) ₂	C ₂₈ H ₃₆ Mn ₂ N ₆ O ₁₆ S ₂	49.6	Yellow	188-189	37.93 (37.88)	4.09 (4.14)	9.48 (9.51)	7.23 (7.27)	12.39 (12.36)
3	[Co ₂ (L)(H ₂ O) ₈](NO ₃) ₂	C ₂₈ H ₃₆ Co ₂ N ₆ O ₁₆ S ₂	65.8	Blue	169-170	37.59 (37.56)	4.06 (4.11)	9.39 (9.42)	7.17 (7.21)	13.18 (13.31)
4	[Ni ₂ (L)(H ₂ O) ₈](NO ₃) ₂	C ₂₈ H ₃₆ Ni ₂ N ₆ O ₁₆ S ₂	59.8	Yellow	177-178	37.61 (37.55)	4.06 (4.11)	9.40 (9.44)	7.17 (7.27)	13.13 (13.22)

Uniform size filter paper disks (3 disks per compound) were impregnated with equal volume (10 µL) from the specific concentration of dissolved tested compounds and then carefully placed on the incubated agar surface. After incubation for 36 hrs at 27 °C in the case of bacteria and for 48 hours at 24 °C in the case of fungi, inhibition of the organisms (evidenced by a clear zone surrounding each disk) was measured and used to calculate the mean of inhibition zones.

2.6. Evaluation of the antitumor activity

The compounds were tested for any cytotoxic activity against the colon carcinoma (HCT-116) cell line. When the cells reached confluence (usually after 24 hrs), the cell suspension of the tumor cell lines was prepared in a complete growth medium (DMEM) supplemented with 50 µg/mL gentamycin [28]. The aliquots of 100 µL of cell suspension (1×10⁵ cell/mL) were added to each plate. The blank wells contained complete medium in place of cell suspension. The cells were incubated for 24 hrs at 37 °C in a humidified incubator with 5% CO₂. After the formation of a complete monolayer cell sheet in each well of the plate, serial two-fold dilutions of the compounds were added into a 96-tissue culture plate using a multichannel pipette (Eppendorf, Germany). The treated and untreated cells were allowed to grow in the presence of test compounds by further incubating the plates for 24 hours. The plates were covered with a plate sealer and then incubated at 37 °C. To obtain quantitative cytotoxicity data, the cells were strained with a 0.1% crystal violet solution. The dye was extracted from the cells by adding glacial acetic acid (33%) to each well and mixing the contents of each well before reading the color absorbance on the ELISA reader (Sunrise TECAN Inc., USA) at 490 nm. The absorbance is proportional to the number of surviving cells. Each experiment was made in quadruplicate and repeated three times. In addition to the cell growth, the inhibition (IC₅₀) ratio was calculated from the absorbance values using the formula: IC₅₀ = (C-T/C)×100, where C is the mean absorbance value of untreated (control) cells and T is the mean absorbance values of treated cells [29,30].

2.7. Cytotoxicity assay

Cell toxicity was monitored by determining the effect of silver nanoparticles on cell morphology and cell viability [31]. The cytotoxicity assay was monitored on VERO cells using 0.1 mL of cell suspension, involving 10,000 cells seeded in each well of a 96-well microtitre plate (Falcon, NJ, USA). Fresh maintenance medium containing different dilutions of the test sample was added after 24 hours of seeding. Control cells were incubated without a test sample. The microtitre plates were incubated at 37 °C in a humidified incubator with 5% CO₂ for a period of 48 hrs. Six wells were used for each concentration of the test sample. After incubation, the culture supernatant was replaced by fresh medium. The cells in each well were then stained and analyzed as described in the antitumor section. The absorbance was detected at 490 nm using a microplate ELISA reader (Sunrise TECAN Inc. USA). The absorbance of untreated cells was considered as 100%.

The cell cytotoxic effect (CC₅₀) of each tested compound was calculated using the following formula: percentage of cell cytotoxic effect = [1-(ODt/ODc)]×100%, where ODt and ODc indicate the absorbance of the test substance and the cell control; respectively.

2.8. Docking and molecular modeling

Thymidylate synthase and dihydrofolate reductase are among the main targets involved in anticancer and antimicrobial activity [32,33]. A molecular modeling study using the Molecular Operating Environment (MOE) [34] module was performed in order to rationalize the observed anticancer activity of APT, H₂L and Ag(I), Mn(II) and Ni(II) complex. Molecular docking studies further helped in explaining the mode of action of the compounds through their various interactions with the active sites of the dihydrofolate reductase (DHFR) enzyme.

Docking and molecular modeling calculations were carried out in the Faculty of Pharmacy, Alexandria University, Egypt. All of the molecular studies were carried out on an Intel Pentium 1.6 GHz processor, 512 MB memory, with a Windows XP operating system, using Molecular Operating Environment (MOE 2005.06; Chemical Computing Group, Montreal, Canada) as the computational software. All of the minimizations were performed with MOE until a RMSD gradient 0.05 Kcal/mol-Å with MMFF94X force field and the partial charges were automatically calculated.

The coordinates of the X-ray crystal structure of methotrexate (MTX) were bound to dihydrofolate reductase (DHFR) enzyme (PDB ID: 4DFR). Enzyme structures were checked for missing atoms, bonds and contacts. Hydrogen atoms were added to the enzyme structure. Water molecules and bound ligands were manually deleted. The ligand molecule was constructed using the builder molecule and was energy minimized. The active sites were generated using the MOE-Alpha site finder. Dummy atoms were created from the obtained alpha spheres. Compounds were docked within the dihydrofolate reductase active sites using the MOE-Dock with simulated annealing used as the search protocol and a MMFF94X molecular mechanics force field for 8000 interactions. The lowest energy conformation was selected and subjected to energy minimization using the MMFF94X force field.

3. Results and discussions

3.1. Characterization of the H₂L ligand and its metal complexes

The structure of the dibasic Schiff base ligand with two NO bidentate sites, and was identified by elemental analysis, melting point, infrared, UV-Visible, ¹H NMR and mass spectrum (Figure 1) and fits with the data cited in the literature [20]. The ligand reacted with Ag(I), Mn(II), Co(II) and Ni(II) ions to yield the corresponding binuclear transition metal complexes. Table 1 lists the physical and analytical data of the metal complexes of the H₂L ligand.

Table 2. Characteristic infrared frequencies (cm^{-1}) of hydrazone, H_2L , ligand and its metal complexes*.

Ligand/Complexes	$\nu(\text{OH})$	$\nu(\text{CH})_{\text{arom}}$	$\nu(\text{CH})_{\text{aliph}}$	$\nu(\text{C}=\text{N})$	$\delta(\text{H}_2\text{O})$	$\nu(\text{M}-\text{O})$	$\nu(\text{M}-\text{N})$	Other bands
H_2L	3400-3166 m, br	3050 w	2990 w	1629 vs	-	-	-	-
$[\text{Ag}_2(\text{L})(\text{H}_2\text{O})_4]$	3410-3291 m, br	3140 w	2976 w	1613 vs	1697 vs	542 w	456 w	-
$[\text{Mn}_2(\text{L})(\text{H}_2\text{O})_6](\text{NO}_3)_2$	3390-3320 m, br	3100 w	2900 w	1620 vs	1689 vs	579 w	439 w	NO_3^- (ionic) 1751, 1382, 839
$[\text{Co}_2(\text{L})(\text{H}_2\text{O})_6](\text{NO}_3)_2$	3370-3301 m, br	3099 w	2850 w	1584 vs	1640 vs	542 w	456 w	NO_3^- (ionic) 1748, 1382, 856
$[\text{Ni}_2(\text{L})(\text{H}_2\text{O})_6](\text{NO}_3)_2$	3380-3315 m, br	3100 w	2930 w	1580 vs	1633 vs	579 w	459 w	NO_3^- (ionic) 1742, 1383, 855

* ν , stretching; δ , bending; vs = very strong; s = strong; m = medium; w = weak; br = broad.

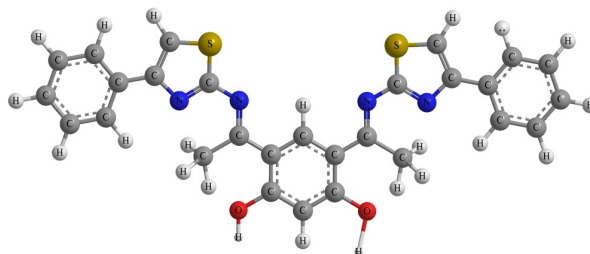
Table 3. Characteristic electronic transition bands and magnetic moments of the metal complexes of H_2L ligand.

Compound	Electronic transition; λ_{max} ; ϵ_{max} , nm ^a		$d-d$ transition		Assignment	μ_{eff} (B.M.) ^b	Λ^c
	$^1\text{L}_a \rightarrow ^1\text{A}$ (Aromatic ring)	$\pi \rightarrow \pi^*$	$^1\text{L}_b \rightarrow ^1\text{A}$ (Aromatic ring)	$n \rightarrow \pi^*$			
H_2L	272 (0.73)	324 (0.83)	335 (0.48)	417 (0.55)	-	-	14
$[\text{Ag}_2(\text{L})(\text{H}_2\text{O})_4]$	272 (0.73)	318 (0.79)	336 (0.55)	-	-	-	22
$[\text{Mn}_2(\text{L})(\text{H}_2\text{O})_6](\text{NO}_3)_2$	272 (0.75)	318 (0.80)	336 (0.48)	408 (0.37)	998 (0.21) 666 (0.28)	$^6\text{A}_{1g} \rightarrow ^4\text{T}_{2g}(^4\text{G})$ $^6\text{A}_{1g} \rightarrow ^4\text{T}_{1g}(^4\text{G})$	6.83 148
$[\text{Co}_2(\text{L})(\text{H}_2\text{O})_6](\text{NO}_3)_2$	272 (0.85)	317 (0.38)	337 (0.38)	409 (0.49)	1061 (0.089) 685 (0.260) 514 (0.122)	$^4\text{T}_{1g}(\text{F}) \rightarrow ^4\text{T}_{2g}(\text{F})$ $^4\text{T}_{1g}(\text{F}) \rightarrow \text{A}_{2g}(\text{F})$ $^4\text{T}_{1g}(\text{F}) \rightarrow ^4\text{T}_{1g}(\text{P})$	4.90 154
$[\text{Ni}_2(\text{L})(\text{H}_2\text{O})_6](\text{NO}_3)_2$	272 (0.87)	315 (0.74)	335 (0.49)	412 (0.43)	1000 (0.083) 625 (0.57)	$^3\text{A}_{2g} \rightarrow ^3\text{T}_{2g}$ $^3\text{A}_{2g} \rightarrow ^3\text{T}_{1g}(\text{F})$	3.21 145

^a Electronic spectra in the visible region recorded in DMF and the values of ϵ_{max} are in parentheses and multiplied by 1×10^{-4} ($\text{mol}^{-1}\text{cm}^{-1}$).

^b The magnetic moment was calculated for one metal ion in the complex.

^c Molar conductance ($\Omega^{-1}\text{cm}^2\text{mol}^{-1}$) was measured in (1×10^{-3} $\text{mol}^{-1}\text{cm}^{-1}$) in DMF solvent.

**Figure 1.** Molecular modelling of the Schiff base, H_2L , ligand.

The geometrical structures of the complexes were identified and characterized using elemental analyses and infrared, UV-visible, mass spectral data. Also, TGA, magnetic susceptibility and molar conductivity measurements were conducted to provide further proofs in identifying the structures.

3.1.1. Infrared spectra

The characteristic vibrational frequencies and their tentative assignments for the H_2L ligand and its transition metal complexes are listed in Table 2. The assignments were aided by comparison with the vibrational frequencies of the free ligand and its related compounds [11,35,36].

The shift of the stretching frequencies of the azomethine $\nu(\text{C}=\text{N})$ group of the metal complexes to lower frequencies that lie in the range of $1620\text{--}1580\text{ cm}^{-1}$, compared with the free ligand band at 1629 cm^{-1} , may be due to the coordination of the two azomethine groups to metal ions [11,35]. The broad bands in the range of $3410\text{--}3291\text{ cm}^{-1}$ are assigned to the stretching frequencies of the $\nu(\text{OH})$ of the water molecules associated to the complexes which are also confirmed by the elemental analyses and TGA data. The weak bands in the two ranges ($579\text{--}542\text{ cm}^{-1}$) and ($459\text{--}439\text{ cm}^{-1}$), are assigned to the stretching frequencies of the $\nu(\text{M}-\text{O})$ and $\nu(\text{M}-\text{N})$ bands, respectively, supporting that the bonding of the ligand to the metal ions is achieved by the phenolic oxygen atoms and the azomethine and amine nitrogen atoms of the ligand. The unidentate nitrate group possesses three non-degenerated modes of the vibrations (ν_s , ν_s' and ν_{as}), which appeared at 1409 , 1311 and 810 cm^{-1} . The $\nu_s(\text{NO}_3^-)$ of the unidentate NO_3^- is markedly shifted to lower frequencies compared to that of the free nitrate ($1700\text{--}1800\text{ cm}^{-1}$) [37]. This could be a factor

measuring the covalent bond strength formed due to the transfer of an electron density from NO_3^- to the metal ion. In complexes $\text{Mn}(\text{II})$, $\text{Co}(\text{II})$ and $\text{Ni}(\text{II})$, the NO_3^- ions behave as free ionic groups and do not coordinate with the metal ions where their vibrations appeared at ($1751\text{--}1742\text{ cm}^{-1}$), ($1383\text{--}1382\text{ cm}^{-1}$) and ($856\text{--}839\text{ cm}^{-1}$), respectively. The $\text{Ag}(\text{I})$ complex did not show such vibrational transitions for nitrate ions, where the conductivity measurements showed the non-electrolytic nature of these complexes.

3.1.2. Electronic, magnetic, mass, TGA and molar conductance measurements

It is possible to draw up the electronic transitions and predict the geometry with the aid of magnetic moments of most metal ions. Table 3 lists the characteristic electronic absorption bands, magnetic moments and molar conductance of the H_2L ligand and its metal complexes in DMF solutions. The electronic transitions due to the organic H_2L ligand in the metal complexes, showed the absorption bands of the $\pi \rightarrow \pi^*$ and $n \rightarrow \pi^*$ transitions results from the $\text{C}=\text{N}$ and $\text{C}=\text{C}$ groups and appeared at $324\text{--}315$ and $412\text{--}408\text{ nm}$ regions, respectively. These values are lower than the corresponding absorption bands for the H_2L ligand, which were observed at 324 and 417 nm , respectively. This may be due to the coordination of the nitrogen and oxygen atoms of the ligands to the metal ions. Also, other two bands were observed in all electronic spectra of the complexes, which persist at the same positions compared to the electronic spectra of the free H_2L ligand, which are the two bands due to the $^1\text{L}_a \rightarrow ^1\text{A}$ and $^1\text{L}_b \rightarrow ^1\text{A}$ transitions of the phenyl ring transitions which were observed at $273\text{--}272$ and $337\text{--}334\text{ nm}$, respectively.

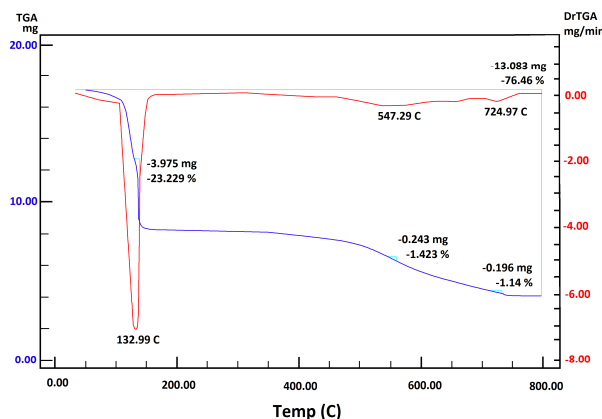


Figure 2. TGA-DrTGA curves of the $[\text{Ni}_2(\text{L})(\text{H}_2\text{O})_8](\text{NO}_3)_2$ complex.

The electronic spectrum of the yellow Mn(II) complex showed two bands at 15015 and 19011 nm. These bands may be assigned to the ${}^6\text{A}_{1g} \rightarrow {}^4\text{T}_{1g}({}^4\text{G})$ (v_3) and the ${}^6\text{A}_{1g} \rightarrow {}^4\text{T}_{2g}({}^4\text{G})$ (v_2) transitions, in order of increasing energy. The third band due to the ${}^6\text{A}_{1g} \rightarrow {}^4\text{A}_{1g}, {}^4\text{E}_g({}^4\text{G})$ (v_1) transition lies in the range of the ligand transitions and is not possible to identify. The magnetic moment was measured and gives 6.83 B.M. This value refers to the fact the Mn(II) complex has high spin octahedral geometry [38].

The electronic spectrum of the blue Co(II) complex in DMF solution showed the complex has an octahedral geometry. Two bands were observed in the visible region, the former one is due to ${}^4\text{T}_{1g}(\text{F}) \rightarrow {}^4\text{A}_{2g}(\text{F})$ (v_2) transition, which is observed at 14600 cm^{-1} . The second band due to ${}^4\text{T}_{1g}(\text{F}) \rightarrow {}^4\text{T}_{1g}(\text{P})$ (v_3) transition is observed at 19470 cm^{-1} . The third near infrared band at 9430 cm^{-1} was assigned to ${}^4\text{T}_{1g} \rightarrow {}^4\text{T}_{2g}$ transition (v_1). The Co(II) complex showed the magnetic moment at 4.90 B.M. at room temperature, where the usual octahedral complexes are around 4.8-5.2 B.M [39]. The crystal field parameter Δ_o and the Racah interelectron repulsion constant B can be easily calculated from the expressions:

$$\Delta_o = v_2 - v_1 \quad (1)$$

$$3B = \frac{(v_2 - 2v_1)(v_1)}{(9v_1 - 4v_2)} \quad (2)$$

which gave 4870 cm^{-1} and 506 cm^{-1} , respectively. The metal Co(II) d -electrons will be partly shared by the ligand. The covalence character can be evaluated from the free ion of Co(II) which has $B = 970\text{ cm}^{-1}$ [40]. Thus, the expression $\beta = B/B_0 = 0.522$, indicates the covalent interaction between the ligand to Co(II) in the complex.

The electronic spectrum of the yellow Ni(II) complex showed two bands at 10000 and 16000 cm^{-1} which are assigned to ${}^3\text{A}_{2g} \rightarrow {}^3\text{T}_{2g}$ (v_1) and ${}^3\text{A}_{2g} \rightarrow {}^3\text{T}_{1g}(\text{F})$ (v_2) transitions in their d^8 octahedral geometry. The measured value of the magnetic moment for Ni(II) complex was 3.21 B.M., which confirms the octahedral structure [41,42]. The third ${}^3\text{A}_{2g} \rightarrow {}^3\text{T}_{1g}(\text{P})$ v_3 transition was obscured from the charge transfer of the organic ligand. The values of v_3 and the crystal field parameter Δ_o and the Racah interelectron repulsion constant B can be easily calculated from the expressions [43]:

$$\Delta_o = v_1 \quad (3)$$

$$3B = \frac{(v_2 - 2v_1)(v_2 - v_1)}{(5v_2 - 9v_1)} \quad (4)$$

$$15B = v_3 + v_2 - 3v_1 \quad (5)$$

which gave 10000 , 800 and 26000 cm^{-1} , respectively. The metal Ni(II) d -electrons will be partly shared by the ligand; i.e., will spend $< 100\%$ of their time on the metal. This can be evaluated from the free ion of Ni(II) which has $B = 1080\text{ cm}^{-1}$ [40]. Thus, the expression $\beta = B/B_0 = 0.741$.

Thermal gravimetric analysis (TGA) of complex was performed to provide further proof in identifying the structure, which shows three stages. The first stage is due to the loss of eight coordinated water molecules (weight loss; Calcd./Found%; 16.11/16.31%) observed at $100\text{-}160\text{ }^\circ\text{C}$. The second stage was observed at $480\text{-}610\text{ }^\circ\text{C}$ and is due to the loss of 2NO_2 molecules (weight loss; Calcd./Found%; 10.29/10.36%). The third stage was observed at $650\text{-}800\text{ }^\circ\text{C}$ and is due to the dissociation of the organic ligand moiety within the complex (weight loss; Calcd./Found%; 56.82/ 56.72%). The residue was 2NiO (weight loss; Calcd./Found%; 16.79/17.07%). Figure 2 depicts the TGA-DrTGA curves of $[\text{Ni}_2(\text{L})(\text{H}_2\text{O})_8](\text{NO}_3)_2$ complex.

The values of the molar conductivity for all complexes were measured at $22\text{ Ohm}^{-1}\text{cm}^2\text{mol}^{-1}$, for Ag(I) complex and $145\text{-}154\text{ Ohm}^{-1}\text{cm}^2\text{mol}^{-1}$, for Mn(II), Co(II) and Ni(II) complexes. These values are consistent with the electrolytic and non-electrolytic nature of the complexes with the nitrate anions [44].

From the interpretation of elemental analysis and infrared, electronic spectra and magnetic moments and molar conductivity measurements, as well as, TGA analysis, it is possible to draw up the tentative structures of the transition metal complexes of the Schiff base H_2L ligand. Figure 3 depicts the molecular modeling of the Ag(I), Mn(II), Co(II) and Ni(II) complexes of the Schiff base H_2L ligand.

3.2. Antimicrobial activity

The Schiff base ligand and its metal complexes were evaluated for antimicrobial activity against three strain Gram-positive bacteria (*Staphylococcus aureus* (RCMB 010027), *Streptococcus pneumonia* (RCMB 010010) and *Bacillus subtilis* (RCMB 010067)), three Gram-negative bacteria (*Pseudomonas aeruginosa* (RCMB 010043), *Klebsiella pneumoniae* (RCMB 0010093) and *Escherichia coli* (RCMB 010052)) and the fungi *Aspergillus fumigatus* (RCMB 02568) and *Candida albicans* (RCMB 05036). The obtained antimicrobials are presented in Table 4. The Schiff base ligand was found to be biologically active against the microorganisms. Table 4 also shows all of the metal complexes exhibit antimicrobial activity in one or more strains and this is enhanced when compared with the parent Schiff base.

Table 4. Anti-microbial activity of the H₂L ligand and its metal complexes. ^{a, b}

Compound	Gram-positive Bacteria			Gram-Negative Bacteria			Fungi	
	<i>S. aureus</i> (RCMB 010027)	<i>S. pneumoniae</i> (RCMB 010010)	<i>B. subtilis</i> (RCMB 010067)	<i>P. aeruginosa</i> (RCMB 010043)	<i>K. pneumoniae</i> (RCMB 0010093)	<i>E. Coli</i> (RCMB 010052)	<i>A. fumigatus</i> (RCMB 02568)	<i>C. albicans</i> (RCMB 05036)
	H ₂ L	29.1±0.37	26.2±0.36	28.1±0.63	28.6±0.63	18.4±0.58	29.1±0.37	26.3±0.44
[Ag ₂ (L)(H ₂ O) ₄]	15.2±0.38	14.6±0.58	16.2±0.58	20.6±0.22	25.4±0.29	13.7±0.25	12.6±0.58	13.6±0.58
[Mn ₂ (L)(H ₂ O) ₈](NO ₃) ₂	13.5±0.41	18.0±0.19	15.0±0.63	17.9±0.52	19.3±0.36	12.6±0.34	17.4±0.46	16.0±0.25
[Co ₂ (L)(H ₂ O) ₈](NO ₃) ₂	17.9 ±0.72	16.9±0.44	19.3±0.25	14.4±0.35	18.2±0.19	14.9±0.44	15.6±0.44	16.2±0.58
[Ni ₂ (L)(H ₂ O) ₈](NO ₃) ₂	20.3±0.38	17.6±0.58	17.7±0.43	14.9±0.44	18.2±0.25	20.3±0.38	17.6±0.58	18.2±0.25
St. Control ^c	28.9±0.14	25.3±0.58	26.4±0.34	26.3±0.15	17.3±0.12	27.3±0.44	23.7±0.10	21.9±0.12

^a Mean zone of inhibition in mm±standard deviation (S.D.) beyond well diameter (6 mm) produced on a range of environmentally and clinically pathogenic microorganisms using (5 mg/mL) concentration of tested samples.

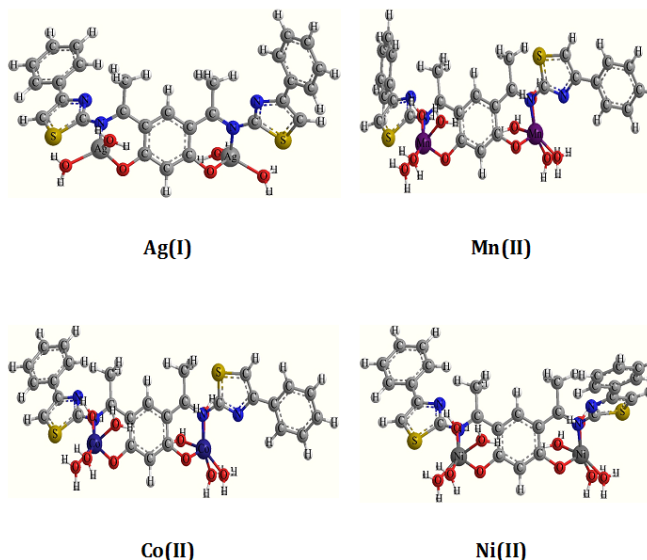
^b The test was performed using the diffusion agar technique. RCMB (Regional Center for Mycology and Biotechnology Antimicrobial Unit Test Organisms).

^c The standard controls for the microorganisms are ampicillin for the Gram-positive bacteria, gentamicin for the Gram-negative bacteria and amphotericin B for the fungi.

Table 5. Evaluation of cytotoxicity against colon carcinoma cells (HCT-116) cell line. ^a

Compound	Validity for sample Conc. (µg/mL)							
	50	25	12.5	6.25	3.125	1.56	0	IC ₅₀
H ₂ L	5.94±0.156	9.21±0.678	13.76±0.354	26.04±0.567	51.39±0.890	68.74±0.821	100	3.30
[Ag ₂ (L)(H ₂ O) ₄]	5.06±0.298	8.85±0.943	12.92±0.456	31.43±0.789	43.32±0.267	57.20±0.932	100	2.37
[Mn ₂ (L)(H ₂ O) ₈](NO ₃) ₂	16.18±0.497	29.72±0.934	41.63±0.321	79.85±0.213	88.64±0.992	94.55±0.289	100	11.10
[Co ₂ (L)(H ₂ O) ₈](NO ₃) ₂	6.98±0.349	12.86±0.930	19.78±0.876	34.64±0.768	49.78±0.987	61.36±0.765	100	3.09
[Ni ₂ (L)(H ₂ O) ₈](NO ₃) ₂	7.54±0.543	13.93±0.589	22.65±0.234	36.74±0.654	54.26±0.432	78.31±0.891	100	3.88
MTX	6.82±0.598	8.89±0.348	14.83±0.560	16.17±0.435	22.28±0.221	34.64±0.456	100	3.21

^a The standard control is methotrexate (MTX). Each value is the mean of three experiments±standard error.

**Figure 3.** Molecular modelling of the Ag(I), Mn(II), Co(II) and Ni(II) complexes.

Although Ag(I) complex showed very high activity as antimicrobial activity, the Mn(II) complex showed a dramatic low activity for all Gram-positive bacteria, and less than the control in Gram-negative bacteria while showing remarkable effect on the fungi.

It is known that chelation tends to make the ligand act as a more powerful and potent bacterial agent. One possible explanation for this increase in activity upon chelation is that, in chelated complexes, the positive charge of the metal is partially shared with donor atoms present on the ligands so there is an electron delocalization over the whole chelated ring. This, in turn, increases the lipid layers of the bacterial membranes. Generally, it is suggested the chelated complexes deactivate various cellular enzymes, which play a vital role in various metabolic pathways of these microorganisms. Other factors which may also explain the increasing biological activity of the metal complexes as compared to the ligand from which they are derived include: solubility, conductivity and dipole moment affected by the presence of metal ions.

3.3. In vitro anticancer studies

The anticancer activity of the newly synthesized H₂L ligand as well as its four metal complexes was investigated on the human colon carcinoma (HCT-116) cell line. Ag(I) and Co(II) complexes with selectivity index (S.I.) = 17.00 and 15.63; respectively, exhibited better activity than the methotrexate (MTX) as a reference drug with S.I. value 13.30, while complexes Mn(II) and Ni(II) with S.I. values 8.59 and 9.30; respectively, were found to be nearly as active as MTX (Tables 5-7). The results revealed that the cytotoxic effects of the H₂L ligand and its metal complexes on normal (VERO) cell lines (Table 6) were significantly different from those on the human colon carcinoma (HCT-116) cell line (Table 5). These findings revealed that Ag(I) and Co(II) required high concentrations to be cytotoxic on normal cells while only low concentrations were enough to produce the same effect on the colon carcinoma (HCT-116) cell line. The significant differences in the compounds' cytotoxicity were supported by the results of

Table 6. Evaluation of cytotoxicity against mammalian cells of African green monkey kidney (VERO) cell line.^a

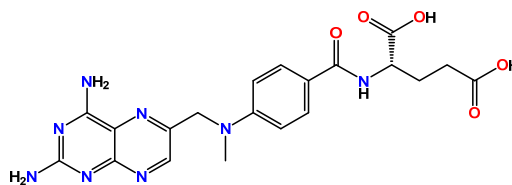
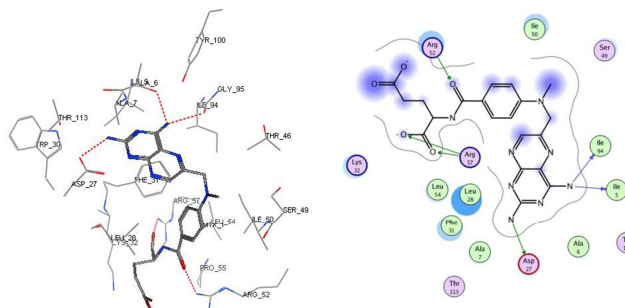
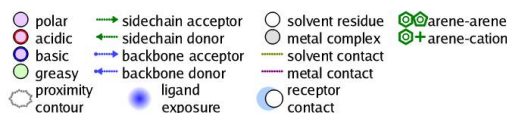
Compound	Validity for sample concentration ($\mu\text{g/mL}$)							CC ₅₀
	50	25	12.5	6.25	3.125	1.56	0	
H ₂ L	19.87±0.543	48.62±0.980	74.83±0.256	83.22±0.634	91.74±0.239	97.31±0.393	100	24.30
[Ag ₂ (L)(H ₂ O) ₄]	41.74±0.908	62.96±0.102	74.54±0.367	88.12±0.746	93.76±0.333	98.24±0.352	100	40.30
[Mn ₂ (L)(H ₂ O) ₆](NO ₃) ₂	80.61±0.237	89.53±0.167	94.36±0.578	98.62±0.120	100.0±0.246	100.0±0.942	100	95.40
[Co ₂ (L)(H ₂ O) ₆](NO ₃) ₂	49.30±0.772	59.72±0.699	75.38±0.756	87.53±0.745	94.81±0.238	98.76±0.114	100	48.30
[Ni ₂ (L)(H ₂ O) ₆](NO ₃) ₂	40.91±0.445	57.23±0.576	69.47±0.834	81.54±0.634	90.08±0.123	94.71±0.350	100	36.10
MTX	42.33±0.590	77.54±0.756	83.05±0.328	90.75±0.439	100.0±0.489	86.10±0.423	100	42.70

^a The standard control is methotrexate (MTX). Each value is the mean of three experiments±standard error.

Table 7. Cytotoxicity of colon carcinoma (HCT-116) cell line and mammalian cells of African green monkey kidney (VERO) cell line on the H₂L and its metal complexes.^a

Compound	CC ₅₀ ($\mu\text{g/mL}$)	CC ₅₀ (μM)	IC ₅₀ ($\mu\text{g/mL}$)	IC ₅₀ (μM)	S.I.
H ₂ L	24.30	47.65	3.30	6.47	7.36
[Ag ₂ (L)(H ₂ O) ₄]	40.30	50.63	2.37	2.97	17.00
[Mn ₂ (L)(H ₂ O) ₆](NO ₃) ₂	95.40	107.67	11.10	12.53	8.59
[Co ₂ (L)(H ₂ O) ₆](NO ₃) ₂	48.30	54.03	3.09	3.46	15.63
[Ni ₂ (L)(H ₂ O) ₆](NO ₃) ₂	36.10	40.38	3.88	4.34	9.30
MTX	42.70	94.05	3.21	7.07	13.30

^a The inhibitory activity against colon carcinoma (HCT-116) cell line was detected under for (50, 25, 12.5, 6.25, 3.125, 1.56 and 0.00 μg) samples concentrations. The cytotoxic activity against mammalian cells of African green monkey kidney (VERO) cell line was detected under for (50, 25, 12.5, 6.25, 3.125, 1.56 and 0.00 μg) samples concentration.

**Structure 1.** Representative structure of the methotrexate (MTX), which bound to the dihydrofolate reductase (DHFR) enzyme.**Figure 4.** Docking of the MTX in the active site of the DHFR. The keys for the type of interactions between the substrate and the DHFR are depicted in Scheme 1.**Scheme 1.** Representative keys for the type of interactions between the substrates and DHFR.

the selectivity index (SI), which is the ratio of the concentration that causes 50% death to African green monkey kidney (VERO) (CC₅₀) to the concentration that causes 50% death to the colon carcinoma cell line (HCT-116) (IC₅₀) [45-47].

3.4. Docking on the active site of dihydrofolate reductase (DHFR)

The recent determination of the three dimensional co-crystal structure of dihydrofolate reductase combined with the potent inhibitor, methotrexate (MTX) (PDB ID: 4DFR) (Structure 1), has led to the development of a model for the topography of the binding site of dihydrofolate reductase. MOE (Molecular Operating Environment) docking studies of the inhibitors were performed using the dihydrofolate reductase

(DHFR) co-crystallized with methotrexate (MTX) (PDB ID: 4DFR) as a template. Scheme 1 thus illustrates the representative keys for the type of interaction between substrates and the DHFR, which can be used as a guide in the docking in Figures 4-7.

Docking of MTX into the DHFR active site revealed that hydrogen bond interactions beside hydrophobic interactions were considered responsible for the observed affinity as it acts as a hydrogen bond donor to the backbone Ile 5 and Ile 94 residues and the side chain Asp 27 residue. It also acts as a hydrogen bond acceptor to Arg 52 and Arg 57 residues. This exists alongside many hydrophobic interactions with various amino acid residues: Ile 5, Ala7, Asp27, Leu 28, Phe 31, Lys 32, Ser 49, Ile 50, Arg 52, Leu 54, Arg 57, Ile 94, Tyr 100 and Thr 113, as shown in Figure 4.

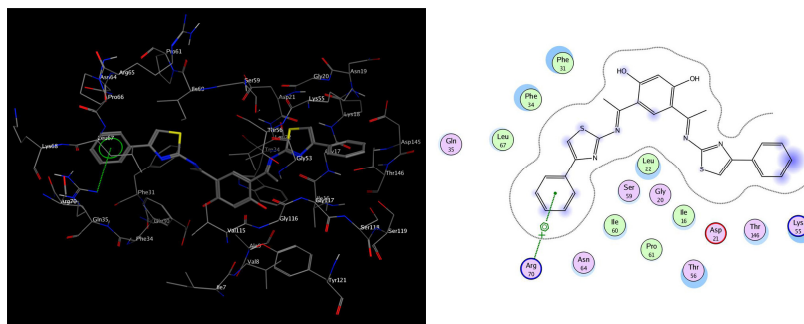


Figure 5. Docking of the H₂L ligand to the active sites of the DHFR. The keys for the type of interactions between the substrate and the DHFR are depicted in Scheme 1.

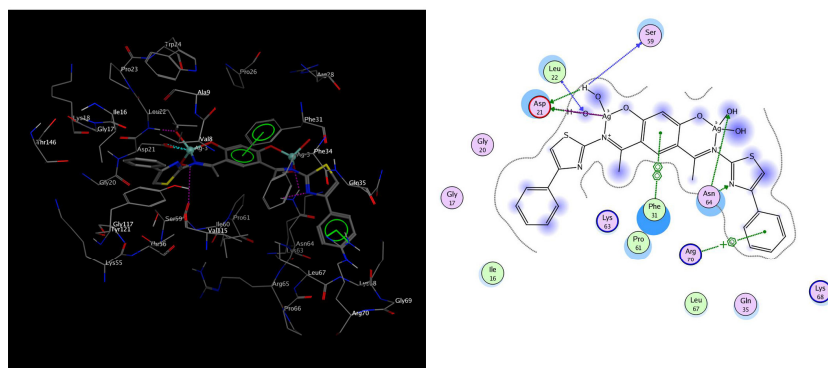


Figure 6. Docking of the Ag(I) complex in the active sites of the DHFR. The keys for the type of interactions between the substrate and the DHFR are depicted in Scheme 1.

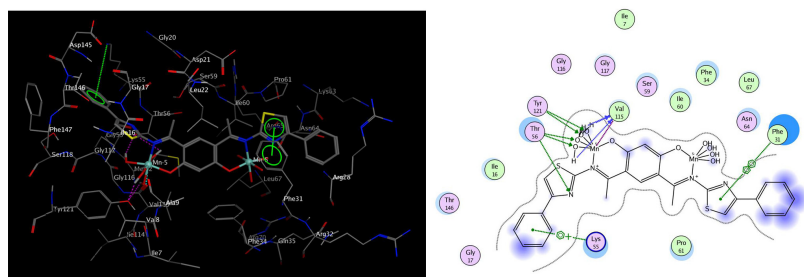


Figure 7. Docking of the Mn(II) complex in the active sites of the DHFR. The keys for the type of interactions between the substrate and the DHFR are depicted in Scheme 1.

Docking of H₂L ligand into the DHFR active site revealed the presence of hydrophobic interactions between almost all atoms in the compound and many amino acid residues: Ile 16, Gly 20, Asp 21, Leu 22, Phe 31, Phe 34, Gln 35, Lys 55, Thr 56, Ser 59, Ile 60, Pro 61, Asn 64, Leu 67, Arg 70 and Thr 146, as shown in Figure 5.

Docking of Ag(I) complex into the DHFR active site revealed the presence of hydrogen bond interaction between the hydroxyl groups as they act as a hydrogen bond donor either with side chain Asp 21 residue (2.56, 3.05 and 1.89 Å) with a strength of 13.7, 1.4 and 3%, respectively; or with the side chain Ser 59 residue (3.67 Å) with a strength of 2%. However, it showed the presence of a hydrogen bond interaction between the oxygen atom of the hydroxyl group as it acts as hydrogen bond acceptor either with side chain Leu 22 residue (2.76 Å) with a strength of 75.8% or with the side chain Asn 64 residue (2.79 and 2.72 Å) with a strength of 1.6 and 52.4%, respectively. Furthermore, it revealed the presence of hydrophobic interactions between other atoms in the

compound and many amino acid residues: Ile 16, Gly 17, Gly 20, Phe 31, Gln 35, Pro 61, Lys 63, Leu 67, Lys 68 and Arg 70, as shown in Figure 6.

Docking of Mn(II) complex into the DHFR active site revealed the presence of hydrogen bond interaction between two oxygen atoms of the four hydroxyl groups, as they act as a hydrogen bond acceptor either with the side chain Thr 56 residue (3.47, 2.69 and 3.40 Å) with a strength of 2.6, 67.6 and 3.7%, respectively; or with the side chain Thr 121 residue (2.36 and 2.68 Å) with a strength of 99 and 87.4%, respectively. Furthermore, it showed the presence of hydrogen bond interaction between the four hydroxyl groups, as they act as a hydrogen bond donor either with the side chain Thr 56 residue (2.69 and 3.40 Å) with a strength of 67.6 and 3.7%; respectively, Val 115 residue (3.17, 3.10 and 0.52 Å) with a strength of 15.8, 19.8 and 46.9%, respectively; or with the side chain Thr 121 residue (2.36 Å and 2.68 Å) with a strength of 99 and 87.4%, respectively.

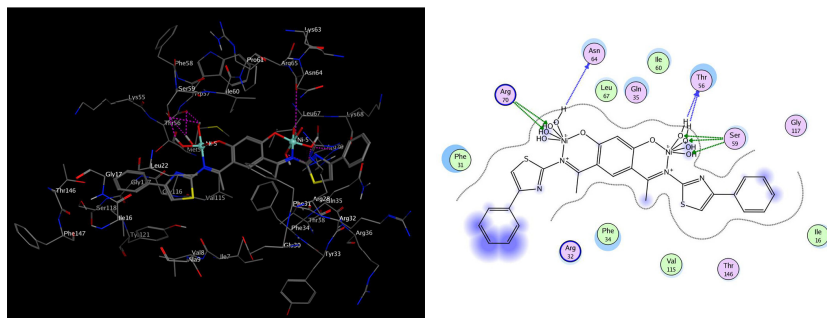


Figure 8. Docking of the Ni(II) complex in the active sites of the DHFR. The keys for the type of interactions between the substrate and the DHFR are depicted in Scheme 1.

In addition, it revealed the presence of hydrophobic interactions concerning other atoms in the compound with many amino acid residues: Ile 7, Ile 16, Gly 17, Phe 31, Phe 34, Lys 55, Ser 59, Ile 60, Pro 61, Asn 64, Leu 67, Gly 116, Gly 117 and Thr 146, as shown in Figure 7.

Docking of Ni(II) complex into the DHFR active site revealed the presence of hydrogen bond interaction between the hydroxyl groups as they act as a hydrogen bond donor either with side chain Thr 56 residue (2.55 and 1.96 Å) with a strength of 7.8 and 57.2%, respectively; Ser 59 residue (3.51, 2.73 and 2.47 Å) with a strength of 1.2, 90.8 and 99.5%, respectively; or Asn 64 residue (3.80 Å) with a strength of 2.5%. However, it showed the presence of a hydrogen bond interaction between the oxygen atom of the hydroxyl group as it acts as hydrogen bond acceptor either with side chain Ser 59 residue (3.51, 2.73 and 2.47 Å) with a strength of 1.2, 90.8 and 99.5 %; respectively or with the side chain Arg 70 residue (3.23, 3.30 and 3.30 Å) with a strength of 10, 9.6 and 6.3%, respectively. Furthermore, it revealed the presence of hydrophobic interactions between other atoms in the compound and many amino acid residues: Ile 16, Phe 31, Arg 32, Phe 34, Gln 35, Ile 60, Leu 67, Gly 117, Val 115 and Thr 146, as shown in Figure 8.

4. Conclusions

The thiazole Schiff base ligand was allowed to react with silver(I), manganese(II), cobalt(II) and nickel(II) ions, with a 1:2 molar ratio (ligand:metal ion). All reactions afforded binuclear complexes for H₂L with either octahedral or tetrahedral geometries. The bonding sites are the azomethine nitrogen atoms and the phenolic oxygen atoms. The ligand and its silver(I) complex enhanced significant antimicrobial activity compared with standard antifungal and antibacterial agents. In the cytotoxicity study, Ag(I) and Co(II) complexes showed the highest inhibitory effects at concentrations that did not affect cellular viability (selectivity index = 17.00 and 15.63; respectively). Docking was performed for the APT, H₂L ligand and the most active anticancer Ag(I), Mn(II) and Ni(II) complexes on the dihydrofolate reductase enzymes in a trial to predict their mode of action as anticancer drugs. The compounds show strong interactions with the dihydrofolate reductase enzyme and mainly Ag(I) and Ni(II) complexes suggest that they might exert their action through inhibition of the DHFR enzyme.

References

- [1]. Abu-Hussein, A. A. *J. Coord. Chem.* **2006**, 59, 157-176.
- [2]. Shebl, M. *Spectrochim. Acta A* **2008**, 70, 850-859.
- [3]. Hobady, M.; Smith, T. D. *Coord. Chem. Rev.* **1973**, 9, 311 -337.
- [4]. Kaim, W.; Schwederski, B. *Bioinorganic Chemistry: Inorganic Elements in the Chemistry of Life*, Wiley, New York, 1994.

- [5]. Atakol, O.; Nazir, H.; Arici, C.; Durmus, S.; Svoboda, I.; Fuess, H. *Inorg. Chim. Acta* **2003**, 342, 295-300.
- [6]. Kita, S.; Furutachi, H.; Okawa, H. *Inorg. Chem.* **1999**, 38, 4038-4045.
- [7]. Chohan, Z. H.; Farooq, M. A.; Scozzafava, A.; Supuran, C. T. *J. Enz. Inh. Med. Chem.* **2002**, 17(1), 1-7.
- [8]. Chohan, Z. H.; Pervez, H.; Rauf, A.; Scozzafava, A.; Supuran, C. T. *J. Enz. Inh. Med. Chem.* **2002**, 17(2), 117-122.
- [9]. Chohan, Z. H.; Rauf, A.; Noreen, S.; Scozzafava, A.; Supuran, C. T. *J. Enz. Inh. Med. Chem.* **2002**, 17(2), 101-106.
- [10]. Valent, A.; Melnik, M.; Hudecova, D.; Dudova, B.; Kivekas, R.; Sundberg, M. R. *Inorg. Chim. Acta* **2002**, 340, 15-20.
- [11]. Emara, A. A.; Abou-Hussen, A. A. *Spectrochim. Acta A* **2006**, 64, 1010-1024.
- [12]. Prajapati, A. K.; Modi, V. P. *J. Chil. Chem. Soc.* **2010**, 55(2), 240-243.
- [13]. Pandeya, S. N.; Mishra, V.; Pandey, A. *Der Pharma Chemica* **2010**, 2(3), 1-7.
- [14]. Pattan, S. R.; Ali, M. S.; Pattan, J. S.; Purohit, S. S.; Reddy, V. V.; Nataraj, B. R. *Indian J. Chem. B* **2006**, 45, 1929-1932.
- [15]. Prakasha, K. C.; Raghavendra, G. M.; Harish, R.; Channegowds, D. *Intl. J. Pharm. Sci.* **2011**, 3(3), 120-125.
- [16]. Kelode, S. R. *J. Chem. Pharm. Res.* **2013**, 5(7), 100-103.
- [17]. Thakar, A. S.; Pandya, K. S.; Joshi, K. T.; Pancholi, A. M. *Eur. J. Chem.* **2011**, 8(4), 1556-1565.
- [18]. Kelode, S. R. *Intl. J. Sci. Engineer. Tech. Res.* **2013**, 2(10), 1800-1803.
- [19]. Joshi, K. T.; Pancholi, A. M.; Pandya, K. S.; Thakar, A. S. *Intl. J. Res. Chem. Environ.* **2011**, 1(2), 63-69.
- [20]. Al-Harbi, S. A.; Bashandy, M. S.; Al-Saidi, H. M.; Emara, A. A. A.; Mousa, T. A. A. *Spectrochim. Acta A* **2015**, 145, 425-439.
- [21]. Flaschka, H. A.; EDTA Titration, 2nd edition, Pergamon Press, New York, 1964.
- [22]. Vogel, A. I. *Textbook of Quantitative Inorganic Analysis*, 4th edition, Longman, London, 1978.
- [23]. West, T. S. *Complexometry with EDTA and Related Reagents*, 3rd edition, DBH Ltd., Pools, London, 1969.
- [24]. Mabbs, F. E.; Machin, D. T. *Magnetism and Transition Metal Complexes*, Dover Publications, New York, 2008.
- [25]. Bauer, A. W.; Kirby, W. W.; Sherris, J. C.; Turck, M. *Am. J. Clin. Pathol.* **1966**, 45, 493-496.
- [26]. Gross, D. C.; De Vay, S. E. *Physiol. Plant Pathol.* **1977**, 11, 13-28.
- [27]. William, H.; Stephen, V. *Theory and Application of Microbiological Assay*, Academic Press; San Diego, 1989.
- [28]. Hay, R. J.; Cleland, M. M.; Durkin, S.; Reid, Y. A. *Cell Line Preservation and Authentication in "Animal Cell Culture"*, (Ed. J. R. W. Masters), Oxford University Press, New York, 2000.
- [29]. Wilson, A. P. *Cytotoxicity and Viability Assays in Animal Cell Culture: A Practical Approach*, 3rd edition, (Ed. J. R. W. Masters), Oxford University Press, New York 2000.
- [30]. Saintigny, Y.; Makienko, K.; Swanson, C.; Emond, M. J.; Monnat, J. R. *Mol. Cell Biol.* **2004**, 2, 6971-6978.
- [31]. Cheng, D.; Yang, J.; Zhao, Y. *Chinese Med. Equip. J.* **2004**, 4, 26-32.
- [32]. Du, Q. R.; Li, D. D.; Pi, Y. Z.; Li, J. R.; Sun, J.; Fang, F.; Zhong, W. Q.; Gong, H. B.; Zhu, H. L. *Bioorg. Med. Chem.* **2013**, 21, 2286-2297.
- [33]. Rao, K. N.; Venkatachalam, S. R. *Bioorg. Med. Chem.* **1999**, 7, 1105-1110.
- [34]. Vilar, S.; Cozza, G.; Moro, S. *Curr. Top. Med. Chem.* **2008**, 8(18), 1555-1172.
- [35]. Emara, A. A.; Saleh, A. I.; Adly, O. I. *Spectrochim. Acta A* **2007**, 68, 592-604.
- [36]. Emara, A. A. *Synth. React. Inorg. Met. Org. Chem.* **1999**, 29, 87-98.
- [37]. Nakamoto, K. *Infrared Spectra of Inorganic and Coordination Compounds*, 5th edition, John Wiley & Sons, New York, 1997.
- [38]. Shah, N. R. *J. Ind. Chem. Soc.* **1981**, 9, 851-854.
- [39]. Greenwood, N. N.; Earnshaw, A. *Chemistry of the Elements*, Pergamon Press, New York, 1989.

- [40]. James E. Huheey, Inorganic Chemistry, Haper Collins College Publisher, New York, 1993.
- [41]. Adly, O. M.; Emara, A. A. *Spectrochim. Acta A* **2014**, *132*, 91-101.
- [42]. Bailar, J. C.; Emeleus, H. J.; Nyholm, R.; Trotman-Dickenson, A. F. Vol. 3, Comprehensive Inorganic Chemistry, Pergamon Press, New York, 1975.
- [43]. Cotton, F. A.; Wilkenson, G. Gaus, P. L. Basic Inorganic Chemistry, John Wiley & Sons, New York, 3rd edition, 1995.
- [44]. Geary, W. J. *Coord. Chem. Rev.* **1971**, *7*, 81-122.
- [45]. Hafidh, R. R.; Abdulmir, A.; Abu Bakar, F.; Jalilian, F. A.; Abas, F.; Sekawi, Z. *BMC Compl. Altern. Med.* **2012**, *12(1)*, 208-218.
- [46]. Chellaian, J. D.; Johnson, J. *Spectrochim. Acta A* **2014**, *127*, 396-404.
- [47]. Suga, A.; Narita, T.; Zhou, L.; Sakagami, H.; Satoh, K.; Wakabayashi, H. *In Vivo* **2009**, *23*, 691-698.